Chapter 2 Morphology and Strength of the Pacific Plate Within the Kermadec Trench

Abstract

Compensation of seafloor topography on the subducting Pacific Plate within the Kermadec Trench is analyzed using a response function technique to determine the effective plate thickness and flexural rigidity within a subduction zone. Swath bathymetry data collected on a 650 km long track parallel to the trench axis on the subducting Pacific Plate within the trench indicate that the effective rigidity and plate thickness may be reduced by extensive faulting of the crust. We observe a series of horst-graben structures which are approximately parallel to the abolute motion of the Pacific plate and oblique to the axis of the trench with relief greater than 1000 m. Assuming that the observed topography is locally compensated and that there is a simple two layer structure for the crust with a strong, thin plate overlying a weak layer, we estimate that the effective plate thickness and flexural rigidity within the trench are 1–2 km and 10^{19}–10^{20} Nm, respectively. An estimate of the flexural rigidity from single track bathymetry and gravity 100 km seaward of the trench is 10^{21} Nm. These values are much lower than estimates for old oceanic lithosphere and support our hypothesis that the strength of the plate decreases within the subduction zone. The spatial variation of the strength of the plate near the subduction zone is an important constraint for dynamic flow models in which lateral variations in rheology have a strong influence on our ability to simulate plate-like behavior and match observed trench morphology.

2.1 Introduction

Generating plate-like motion in convection models of the Earth's mantle reamins an important plroblem in geodynamics. Several studies have shown that by including weak plate margins in viscous flow models, rigid plates with little internal deformation and the observed toroidal component of plate motion can be reproduced [O'Connell et al., 1991; Lithgow-Bertelloni et al., 1993; Bercovici, 1995; Zhong and Gurnis, 1996]. These models use a variety of rheologic laws which lead to weakening at the plate margin on length scales of a few hundred to a thousand kilometers. However, the extent, mechanism, and length scale of weakening of the subducting (and overriding) plate is still unknown. Using observations of gravity and bathymetry parallel to the trench, at increasing distance seaward of the trench, spectral response function methods can be used to constrain length scale and degree of weakening of the subducting plate.

Gravity anomalies on oceanic plates at short to intermediate wavelength (10–500 km) reflect the seafloor topography while at longer wavelengths (>500–1000 km) there is little observed correlation. The difference is due to the mechanism of isostatic compensation, which changes as a function of wavelength. At short wavelengths the elastic strength of the crust supports part of the topography while at longer wavelengths flow within the ductile lithosphere and mantle, and variations in crustal thickness, dominate the nature of the compensation. The gravity anomaly due to topography on the seafloor can be predicted for various models of compensation. The response function expresses the dependence of the gravity anomaly on topography as a function of several physical parameters (plate thickness, crustal density structure, plate rigidity) and wavelength. The response function can be obtained by direct inversion from spectral analysis of observations of gravity and topography providing a method for measuring the physical parameters affecting compensation [Dorman and Lewis, 1970].

The application of the response function technique to determine the flexural rigidity or effective elastic plate thickness has been used to study the flexural response of normal oceanic lithosphere from the ridge crest to abyssal depths [McKenzie and

Bowin, 1976; McNutt, 1979; Cochran, 1979; Watts and Daly, 1981]and the special case of loading of the lithosphere by large seamounts [Watts, 1978; Watts and Daly, 1981]. These studies conclude that elastic thickness T_e of oceanic plates increases with the age of the plate, with values of 5 km near ridge crests and 25–50 km for lithosphere older than 60 Ma. Studies of loading by seamounts conclude that the flexural response is sensitive to the plate thickness at the time of loading.

Deformation of the seafloor within subduction zones has traditionally been studied by modeling the profile of bathymetry perpendicular to a trench as the response to bending of a thin elastic [Watts and Talwani, 1974; Bodine and Watts, 1979] or a viscous [Bremaecker, 1977; Melosh, 1978] plate due to loading at (or beyond) the trench. In these models it is assumed that the strength of the plate, whether it is elastic strength of the crust or viscous strength of the lithosphere, is uniform. Models using an elastic-plastic rheology [Turcotte et al., 1978; Carey and Dubois, 1982] or include variable plate thickness [Judge and McNutt, 1991] are better able to match steep trench profiles (such as the Marianas and Tonga) by reducing the effective strength or elastic thickness of the plate within the trench. However, thin plate models predict bending stresses exceeding the strength of the crust (greater than several kilobars), while bending stresses in the viscous plate model are less than 1 kbar. An important limitation of these models is the assumption of an applied force or moment to the plate, which can not be directly associated with the negative buoyancy of the slab or flow within the mantle that are responsible for the observed deformation.

Here we present response function analysis within the Kermadec Trench. Results using only a single line of bathymetry and free-air gravity data for a 650 km long track within the Kermadec Trench are inconclusive. We find that by averaging over the spectra of several parallel lines of bathymetry from the swath mapping, we can estimate the elastic plate thickness and rigidity within the trench by increasing the signal-to-noise ratio at short to intermediate wavelengths (20–300 km). We compare our results to the analysis of single track data for normal Pacific Plate (south of Hawaii) and the Pacific Plate 100 km seaward of the Kermadec Trench. Although appropriate data sets do not currently exist, the averaging method for the swath

bathymetry may provide a method for estimating the change in effective plate thickness and flexural rigidity as a function of distance from the trench, providing an important constraint on the deformation of the shallow lithosphere within a subduction zone.

2.2 Observations

In October 1998, single track echo-sounder, gravity data and swath bathymetry was collected on the subducting Pacific Plate within the Kermadec Trench using the research vessel ice breaker (R/VIB) *Nathaniel B. Palmer* (cruise NBP9806A) (Figure 2.1). The track was chosen to follow a single contour of depth or gravity anomaly, although the variations in both of these were much larger than expected from previously available bathymetry and gravity. The track segment within the Kermadec Trench extends from south of the Osbourn Seamount (the westernmost seamount of the Louisville seamount chain) at 26°S and a depth of 6000 m to 32°S and a depth of 7000 m. The segment is 650 km long, with an average depth of 7000 m, a maximum depth of 8400 m and average gravity anomaly of −120 mgal. The total relief within the track at wavelengths of ∼100 km is greater than 2000 m with corresponding gravity anomalies 25–50 mgals (Figure 2.2A, B).

Swath bathymetry mapping of the trench wall is shown in Figure 2.3 as a 3-D perspective image and in Figure 2.4 with contours of depth providing a unique view of the bathymetry and deformation of the seafloor within the subduction zone. At each point along the ship-track the swath bathymetry is derived from 120 adjacent measurements (pings) of travel time taking into account variation in sound speed due to temperature at shallow depths and motion of the ship.

Immediately south of the Osbourn Seamount, steep fault scarps appear along the trench wall at depths of 6200 m transitioning to a series of oblique grabens approximately 125 km from the start of the track at a depth of 7500 km. The grabens are each several kilometers wide and are at least as long as the track width (20 km). The grabens are oblique to the axis of the trench, but are perpendicular to the absolute plate motion direction [de Mets et al., 1990]. The trend of abyssal hill

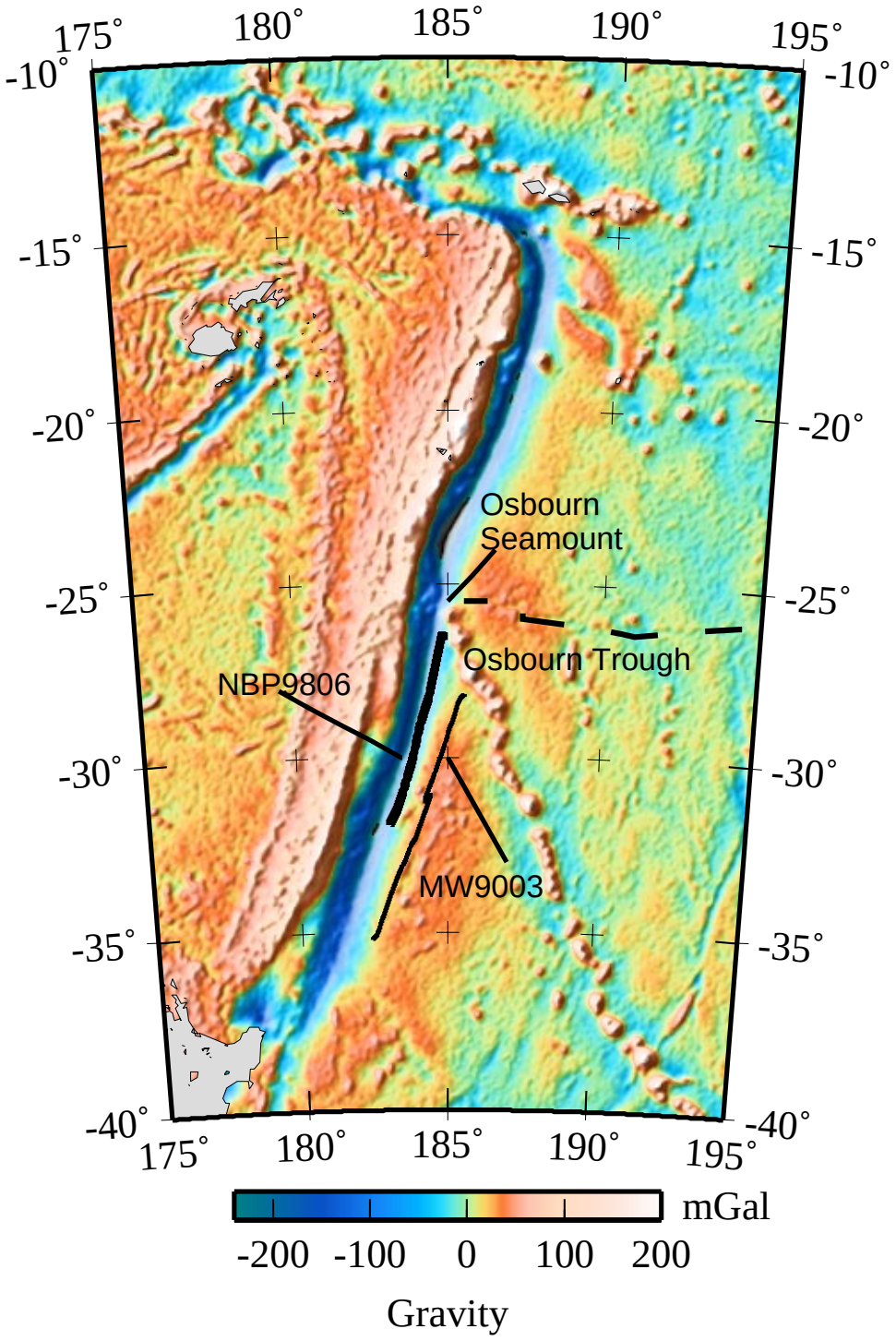

Figure 2.1: Satellite gravity image [Sandwell and Smith, 1997] and location of ship-track segment from cruise NBP9806A (thick solid line) and cruise MW9003 (thin solid line) used in analysis of plate rigidity within the trench. Dashed line marks the location of the extinct spreading center, the Osbourn trough.

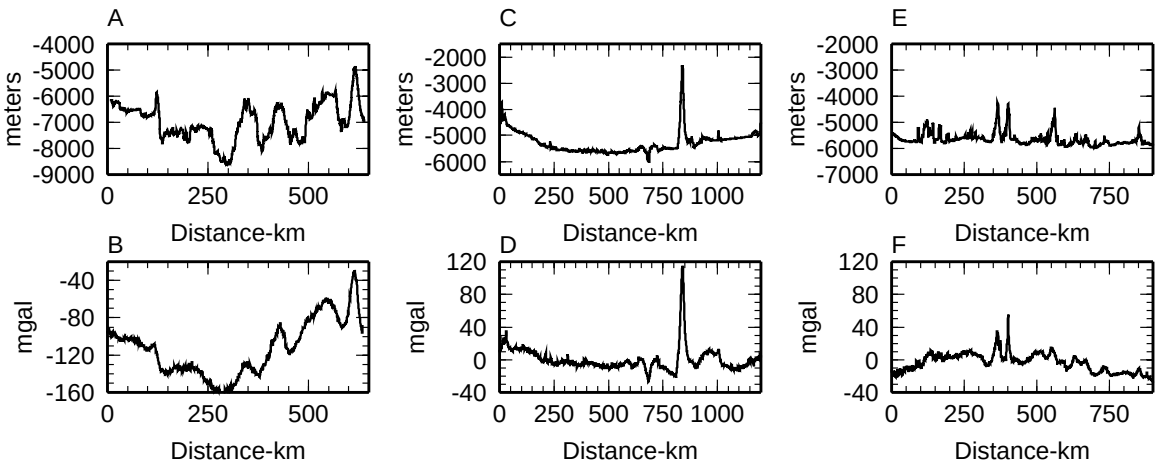

Figure 2.2: **A.** Bathymetry profile on the Pacific Plate within the Kermadec Trench. **B.** Free-air gravity profile for Kermadec Trench ship-track segment. **C.** Bathymetry profile for normal Pacific Plate south of Hawaii (start: 18.9^{o}N,159^{o}W, end: 8.5^{o}N,162^{o}W). **D.** Free-air gravity profile for Pacific Plate ship-track segment. **E.** Bathymetry profile on the Pacific plate 100 km seward of the Kermadec Trench (cruise MW9003). **F.** Free-air gravity profile for MW9003 cruise ship-track segment.

fabric of the subducting plate is almost perpendicular to the trench at the location of the grabens, constrained by the trend of an extinct spreading center, the Osbourn Trough, north of the Osbourn Seamount [Chapter 1]. The series of oblique grabens are observed over a 100 km long section of track transitioning into grabens oriented parallel to the trench axis and extending over 100 km in length and occasionally interrupted by small seamounts.

Near the southern end of the track (31.25°S) a relatively intact shallow region of seafloor appears to be cut by a fault over 50 km long with vertical offset of ∼500 m, while its boundary closer to the trench is marked by a 1500 m drop into an adjacent graben. The central region of the small seamount at 31.75°S appears uncut by faults while the small grabens parallel to the track on either side increase in depth away from the seamount. The change in slope across the seamount in the contour map suggests that these grabens do extend into the seamount with smaller offsets.

Similar seafloor morphology has been observed in several subduction zones, including the Tonga Trench north of the Osbourn Seamount [e.g., Lonsdale, 1986], the Mariana trench [e.g., Ogawa et al., 1997], the Philippine Trench [e.g., Lallemand et al.,

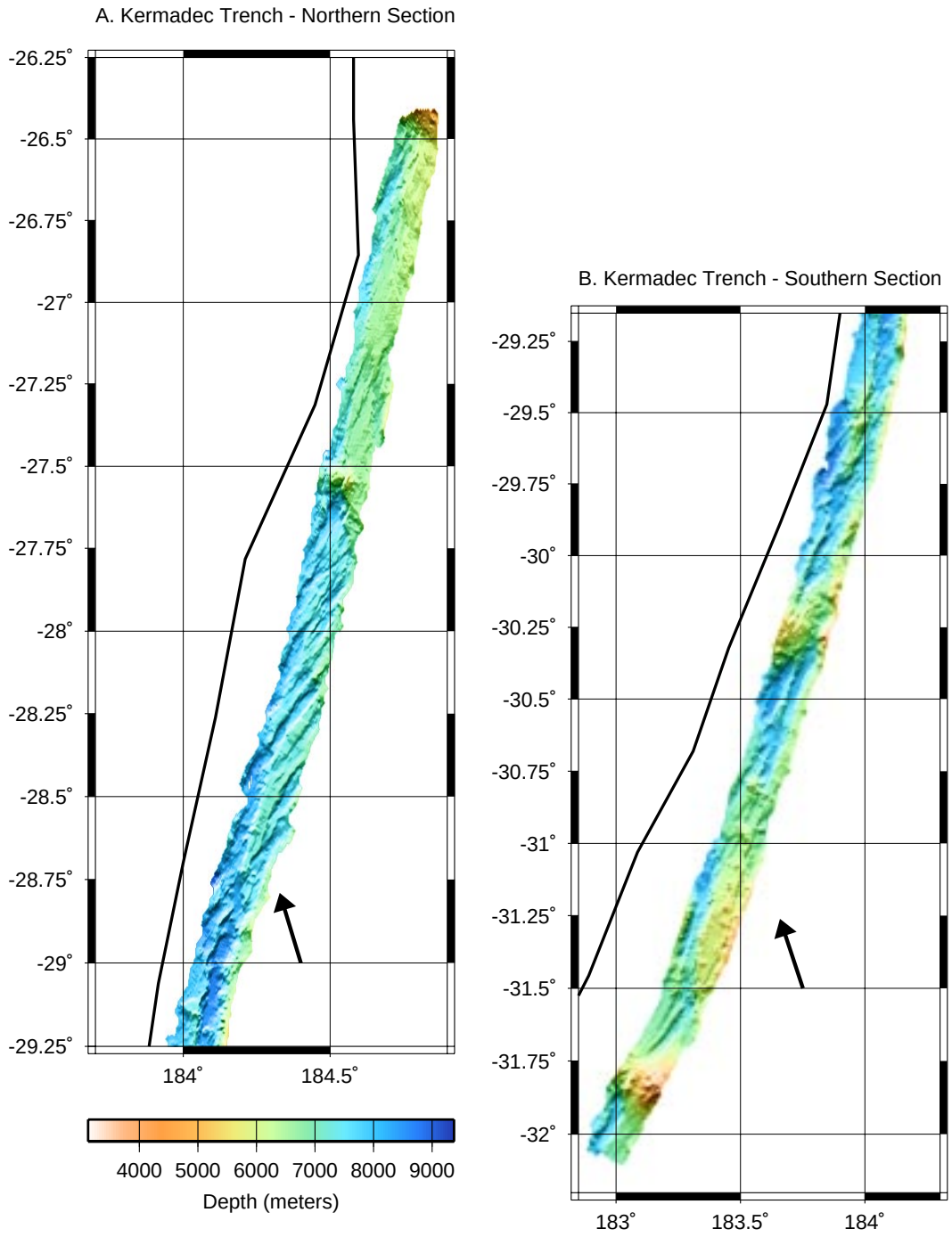

Figure 2.3: 3-D perspective image of Seabeam data within Kermadec Trench. **A.** Northern section of Kermadec Trench beginning immediately south of the Louisville Teamount. The trench axis is to the west. **B.** Southern section of Kermadec Trench, continuation of northern section from 29.25^{o}S. Solid black line marks the trench axis. Black arrow is the absolute plate motion direction of the Pacific Plate from NUVEL-1 [de Mets et al., 1990].

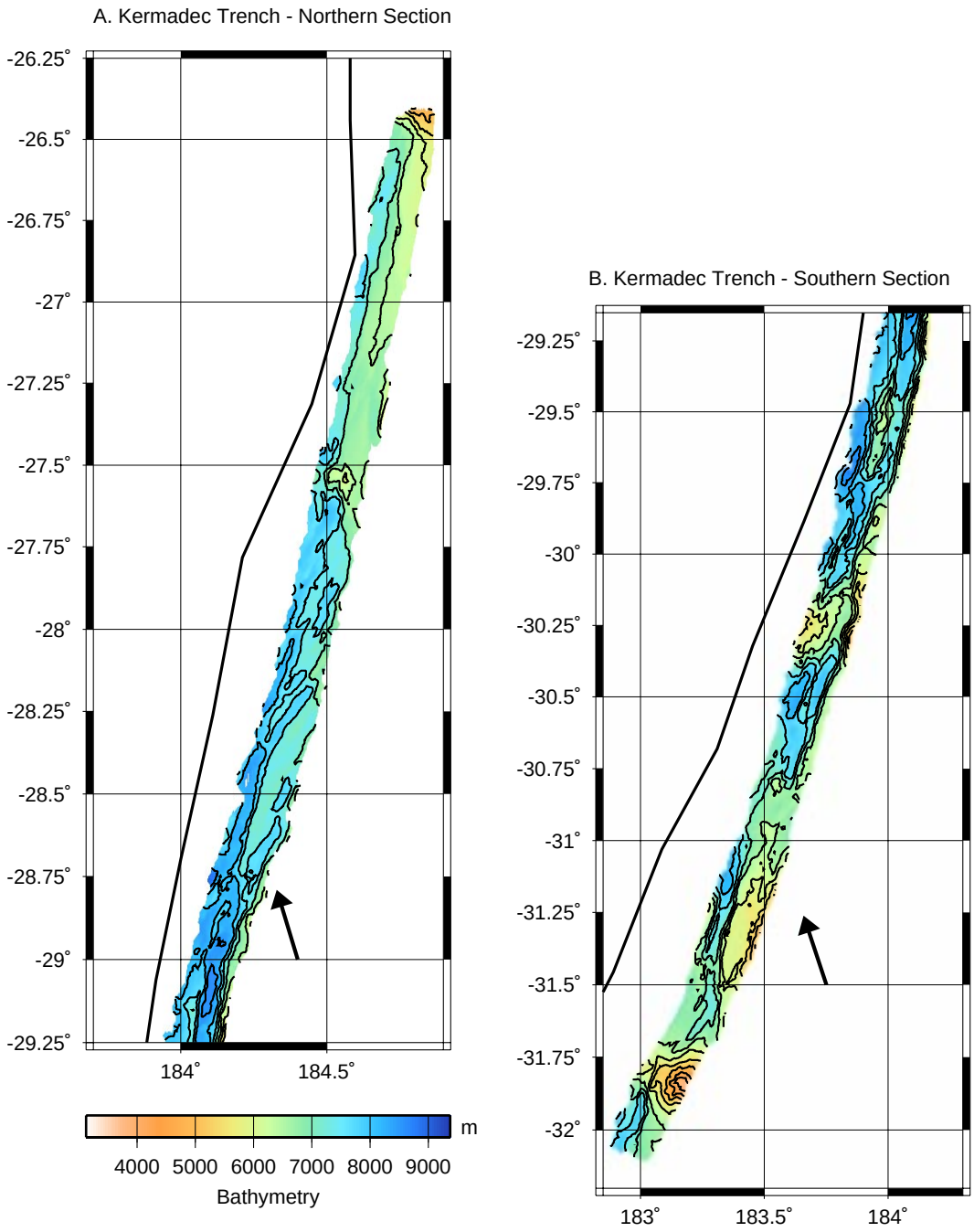

Figure 2.4: Same as Figure 2.3 with contours of Seabeam bathymetry within the Kermadec Trench (contour interval is 500 m). **A.** Northern section of Kermadec Trench beginning immediately south of the Louisville Seamount. The trench axis is to the west. **B.** Southern section of Kermadec Trench, continuation of northern section from 29.25^{o}S. Solid black line marks the trench axis. Black arrow is the absolute plate motion direction of the Pacific Plate from NUVEL-1 [de Mets et al., 1990].

1998], the Japan-Izu-Bonin Trench [e.g., Kobayashi et al., 1987], the Middle America Trench [e.g., Aubouin et al., 1984], Peru-Chile Trench [e.g., Judge and McNutt, 1991; Warsi et al., 1983] and the Aleutian Trench [in Masson, 1991]. Descriptions of faults and horst-graben structures in the outer trench wall indicate that these features trend parallel or sub-parallel to the trench axes. Reactivation of oceanic spreading fabric occurs when this fabric is aligned within 10–20° of the trench axis directions. In cases where the seafloor fabric is perpendicular to the trench, faults are generally aligned parallel to the trench [Masson, 1991].

2.3 Response Function Analysis

Extensive faulting of the subducting plate within the trench indicates that the effective elastic strength may be greatly reduced locally. In order to estimate the strength of the plate within the trench, we use a response function technique to invert for the elastic plate thickness or flexural rigidity from the observations of bathymetry and gravity. Following the analysis of McKenzie and Bowin [1976] and McNutt [1979], we compute the response function from the Fourier transform of gravity $G(k)$ and bathymetry $B(k)$

$$Z(k) = \frac{C(k)}{E_o(k)} \tag{2.1}$$

where $C(k)$ is the cross-spectrum given by

$$C(k) = \frac{1}{N}\sum_{i=1}^{N} G(k)_i B_i^*(k) \tag{2.2}$$

and $E_o(k)$ is the power spectrum of bathymetry

$$E_o(k) = \frac{1}{N}\sum_{i=1}^{N} B(k)_i B_i^*(k) \tag{2.3}$$

and E_1 is the power spectrum of gravity

$$E_1(k) = \frac{1}{N}\sum_{i=1}^{N} G(k)_i G_i^*(k) \tag{2.4}$$

where N is the number of profiles and $*$ denotes the complex conjugate. Although the data is not always available, in the presence of noise and for short transects of data, a better estimate of the response function can be obtained by averaging over several profiles. The Fourier analysis requires that the observations be sampled at equal intervals. A linear interpolation is used to resample the data every 0.5 km along the ship-track, about twice the average sampling rate of the observations. Our analysis is limited to wavelengths of less than 300 km since the total track length is only 650 km. The uncertainty in the admittance, $\delta Z(k)$ is

$$\delta Z(k) = \frac{\sigma(k)}{(E_o(k))^{1/2}} \tag{2.5}$$

$$\sigma^2(k) = \frac{1}{N-1} \sum_{i=1}^{N} (G_i(k) - Z(k)B_i(k))(G_i^*(k) - Z(k)B_i^*(k)) \tag{2.6}$$

In addition to the formal error, for the analysis of multiple pings within the swath bathymetry the coherence

$$\gamma^2(k) = \frac{N(\frac{C(k)C^*(k)}{E_o(k)E_1(k)}) - 1}{(N-1)} \tag{2.7}$$

and the phase of the admittance, ϕ, indicate the wavelengths at which the admittance estimate is robust, i. e., the coherence is high (>0.5) and the phase is small.

It is important to note that in the above analysis it is assumed that the bathymetric load causing the observed gravity extends infinitely in the direction perpendicular to the ship-track. This assumption is not true given our hypothesis that the strength of the plate is decreasing toward the trench and the observation that the faults observed in the seafloor morphology develop within the subduction zone. However for the short–intermediate wavelengths used in our analysis this should not significantly influence the results. In addition, while we believe that the faulting seen in the seafloor morphology at very short wavelengths (5–15 km) reflects weakening of the elastic strength of the plate, our analysis is focused on the compensation of topography at wavelengths greater than 20 km.

The observed response function analysis for a single ping track within the bathymetry

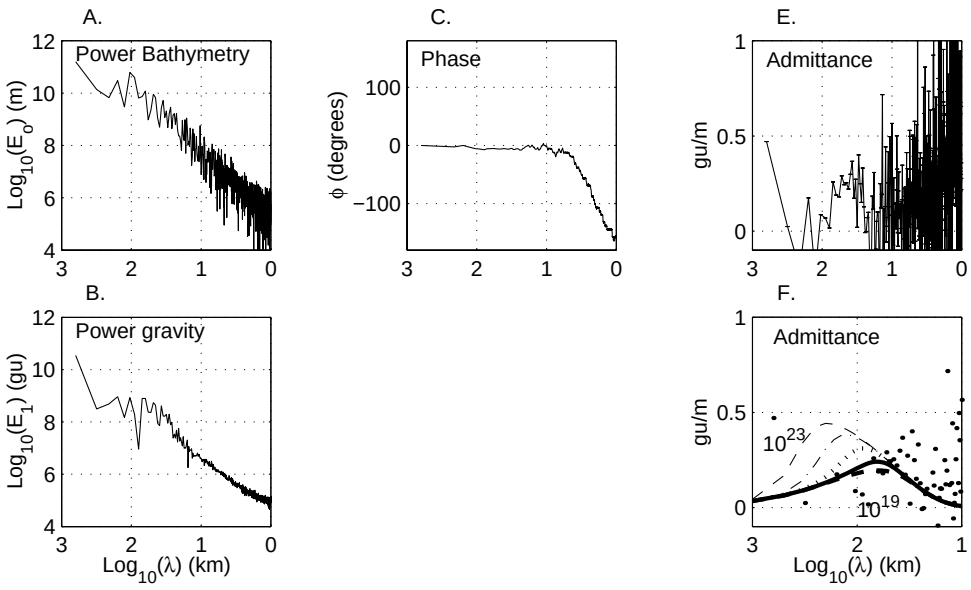

Figure 2.5: Isostatic flexural response within the Kermadec Trench for a single track, from ship-track NBP9806A Seabeam bathymetry and gravity. **A.** Power spectrum of bathymetry (E_o). **B.** Power spectrum of gravity (E_1). **C.** Phase of admittance (ϕ). **D.** Coherence (γ^2), omitted for single track, see text. **E.** Admittance (Z) with uncertainty estimates (δZ). **F.** Admittance estimate (black dots) compared to theoretical curves. Theoretical curves are shown for different values of flexural rigidity D: dashed, 10^{23} Nm; dash-dot, 10^{22} Nm; dotted, 10^{21} Nm; solid-thick, 10^{20} Nm; dashed-thick 10^{19} Nm ($z_1 = 7$ km, $z_2 = 10$ km, $\rho_c = 2400$ kg/m^3).

swath is shown in Figure 2.5 for wavelengths of 1–300 km. A clear peak in the admittance curve occurs at a wavelength of 65 km with a peak value of about 0.25. At wavelengths less than about 50 km the uncertainty in the admittance estimate is indicated by large errors (Figure 2.5E) and increasing phase of the admittance (Figure 2.5F). Note that the coherence is identically equal to one for a single track.

The scatter of the admittance can be reduced by averaging over adjacent tracks within the bathymetry swath (Figure 2.6E). Since multiple ship-track gravity profiles are not available we use gravity profiles from the free-air gravity derived from satellite altimetry [Sandwell and Smith, 1997]. Comparison of the the ship-track gravity profile with the satellite gravity profile shows very good agreement at wavelengths greater than about 5 km. The peak in the admittance curve remains at 65 km while the scatter in the admittance estimates decreases significantly. In addition, the phase is small at all wavelengths and the coherence is high at wavelengths of 20 to 300

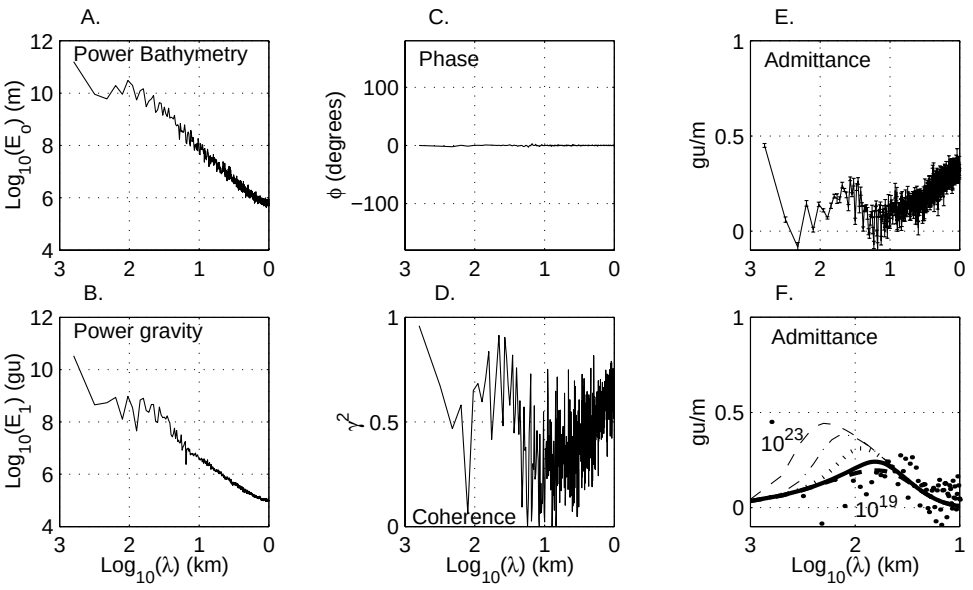

Figure 2.6: Isostatic flexural response within the Kermadec Trench for 80 adjacent pings (30–110), from ship-track NBP9806A Seabeam bathymetry and gravity. See Figure 2.5 for details.

km. The presence of the peak in both the single track and averaged data gives us confidence that this is a robust feature present in the raw data.

For comparison with the admittance estimates within the trench we include analysis of single track data for a 1000 km long section on normal Pacific south of Hawaii (Figure 2.2C, D) from the same cruise (NBP9806A) and for a 1000 km long section of seafloor 100 km seaward of the Kermadec Trench from the University of Hawaii cruise MW9003 [GEODAS, 1992] (Location in Figure 2.1; Profiles in Figure 2.2E, F) shown in Figures 2.7 and 2.8, respectively. While the scatter in the admittance for these two single track data sets is significant, the peak in the admittance curve for the Pacific Plate is clearly at higher wavelengths ($\sim$150 km) with larger values ($\sim$0.5) than the Kermadec Trench admittance. The admittance for the track seaward of the Kermadec Trench is intermediate between the results within the trench and on normal seafloor with at peak around 100 km and peak amplitude at about 0.35.

The observed response function can be compared to the theoretical response function for a model of local compensation by a thin plate with flexural rigidity D, average

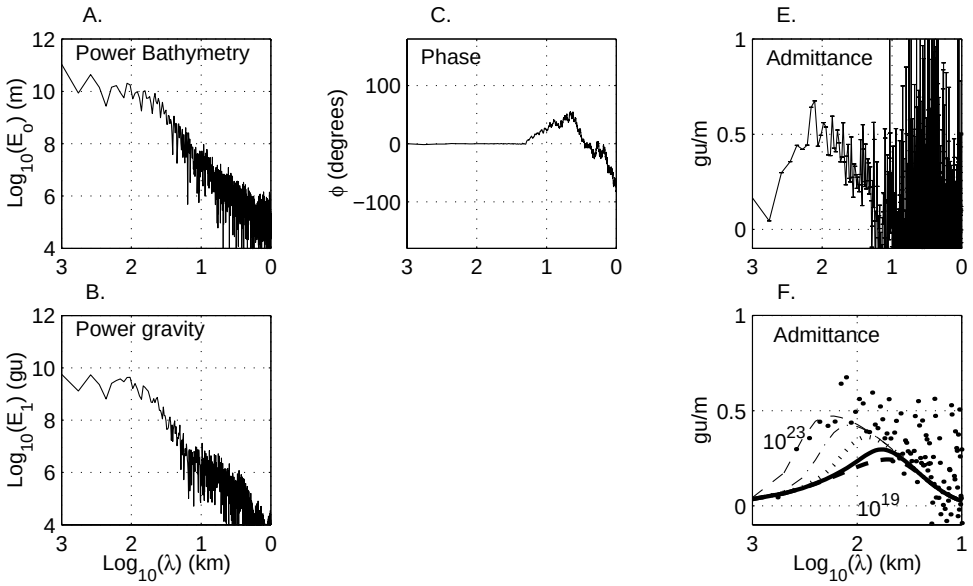

Figure 2.7: Isostatic flexural response for normal Pacific seafloor for a single track, from ship-track NBP9806A Seabeam bathymetry and gravity. ($z_1 = 5$ km, $z_2 = 10$ km, $\rho_c = 2400$ kg/m^3). See Figure 2.5 for details.

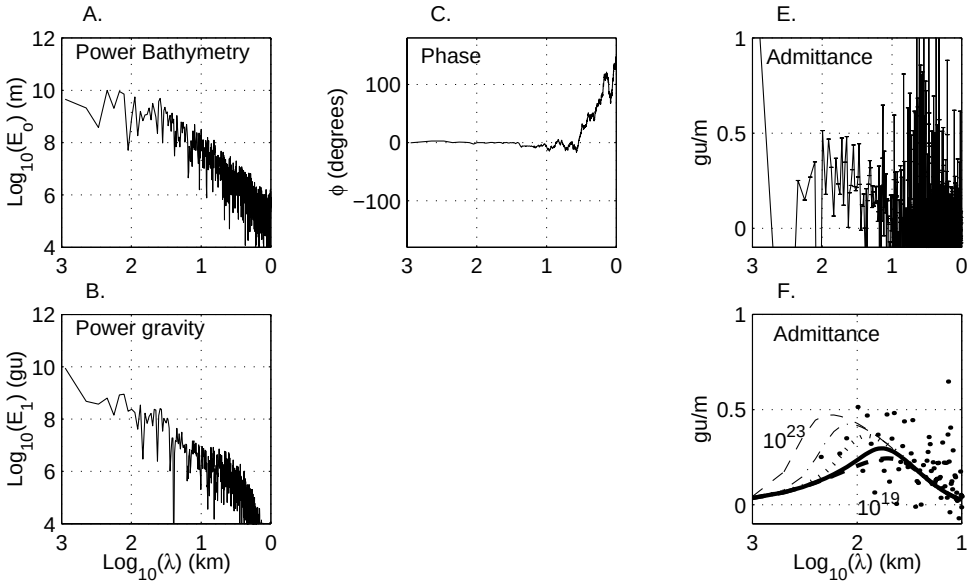

Figure 2.8: Isostatic flexural response for seafloor 100 km seaward of the Kermadec Trench from University of Hawaii cruise MW9003 [GEODAS, 1992] ($z_1 = 5$ km, $z_2 = 10$ km, $\rho_c = 2400$ kg/m^3). See Figure 2.5 for details.

depth to the seafloor z_1, and crustal thickness z_2, overlying a fluid lower lithosphere

$$Z(k) = 2\pi\Delta\rho_c G\times \\ [\exp(-2\pi k z_1) - \Phi(k,D)\exp(-2\pi k z_2)] \tag{2.8}$$

where $\Delta\rho_c = \rho_c - \rho_w$, ρ_c is the crustal density, ρ_w is the density of water, G is the gravitational constant, k is the wavenumber and

$$\Phi(k,D) = \left(1 + \frac{16\pi^4 k^4 D}{\Delta\rho_m g}\right) \tag{2.9}$$

where $\Delta\rho_m = \rho_m - \rho_c$, ρ_m is the mantle density (3300 kg/m^3) and g is the gravitational acceleration. Elastic plate thickness, h_e is related to flexural rigidity by

$$D = \frac{E h_e^3}{12(1-\nu^2)} \tag{2.10}$$

where E is Young's modulus and ν is Poisson's ratio. The depth of compensation (z_2) affects the long wavelength response, decreasing the response function for smaller z_2, while the crustal density affects the amplitude at short wavelengths. The amplitude and wavelength of the response function peak depend on the flexural rigidity.

The predicted response functions for each region are compared to the theoretical curves for five values of flexural rigidity (10^{19}–10^{23} Nm) in Figures 2.5-2.8F. The crustal density is $2400 kg/m^3$, much lower than the density of basalt which may reflect an average density for the observed topography of sediment and basalt [McNutt, 1979]. The crustal thickness is 10 km and the average depth to the seafloor is 7 km within the trench and 5 km for the ship-tracks outside the trench. The estimate of admittance within the Kermadec Trench is best fit with flexural rigidity of 10^{19}–10^{20} Nm while the data 100 km seaward of the trench is best fit by a larger flexural rigidity of 10^{20}–10^{21} Nm. Both of these results are less than the flexural rigidity found for Pacific seafloor far from the trench, 10^{23}–10^{24} Nm.

2.4 Discussion and Conclusions

While there is considerable scatter in the data due to the limited length of the ship-tracks, the response function for the Kermadec trench data is clearly different from the response function for the Pacific Plate far from the trench. The larger flexural rigidity corresponding to an elastic plate thickness of 22–48 km (with $E = 0.6 \times 10^{11}$ Pa and $\nu = 0.25$) agrees with previous results for lithosphere older than 60 Ma. In contrast the response function for the subducting Pacific Plate within the Kermadec Trench, with an age of approximately 100 Ma [Chapter 1], is best matched by a much smaller elastic plate thickness of 1–2 km. The intermediate value of the flexural rigidity for the seafloor 100 km seaward of the Kermadec Trench corresponds to an elastic plate thickness of 4–10 km, also smaller than expected for lithosphere of this age. This estimate for elastic plate thickness 100 km seaward of the trench is similar to estimates for the Chile trench where the elastic plate thickness is estimated to decrease by a factor of two [Judge and McNutt, 1991] trenchward of the forebulge. The lower values within the trench indicate that progressive faulting of the subducting plate trenchward of the forebulge may reflect continual weakening of the elastic strength of the plate extending several hundreds of kilometers from the trench axis.

While both elastic plate models and viscous models of trench topography are able to reproduce trench morphology, constraining the spatial extent and magnitude of the decrease in elastic strength will provide insight into the degree to which trench topography is supported elastically by the upper lithosphere versus viscously by the lower lithosphere. These preliminary results suggests that there is little elastic strength within the trench and forebulge and therefore trench morphology is supported by viscous forces within the lithosphere.

The apparent decrease in the elastic strength of the lithosphere may be caused in part by fracturing of the shallow portion of the crust occurring as the plate at the surface responds to bending stresses transmitted to the surface along the subducting slab. Conrad and Hager [1999] demonstrated that bending and unbending of the subducting lithosphere within a subduction zone leads to large amounts of viscous dissipation along the top and bottom boundaries of the subducting lithosphere ex-

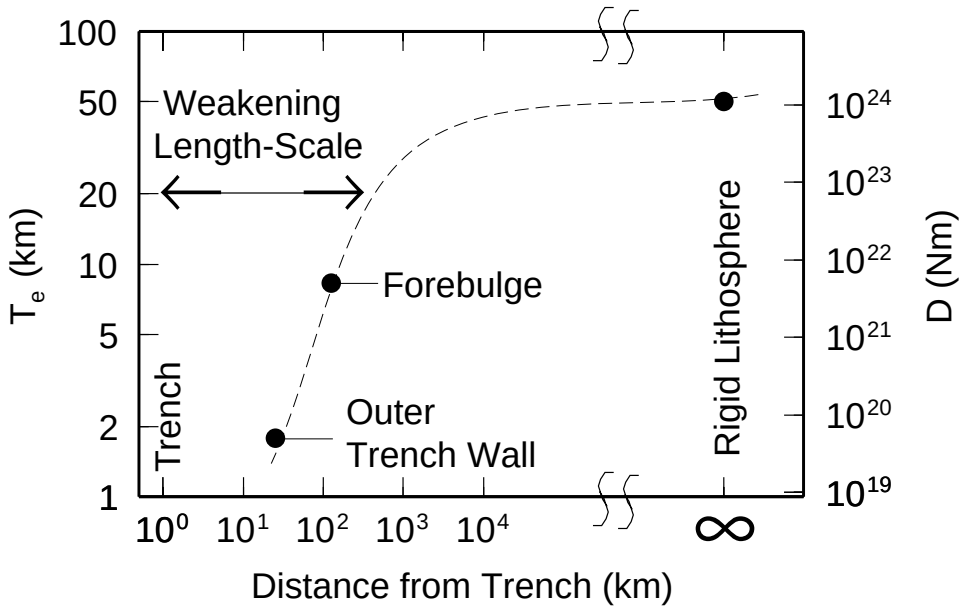

Figure 2.9: Schematic for drop in lithospheric strength at convergent plate boundaries. The three circles are estimates of flexural rigidity of elastic plate thickness from this study, where the point for normal oceanic lithosphere represents the rigid lithosphere. The dashed curve represents a possible weakening behavior for the subducting lithosphere. Further measurements are needed to determine the true weakening behavior.

tending greater than 200 km from the trench axis, and that this dissipation plays an important role in regulating plate velocities.

Measurement of the width over which the elastic strength decreases seaward of the trench provides an important constraint for dynamic models of convection and surface deformation. Figure 2.9 shows schematically how measurement of plate rigidity at increasing distance from the trench would constrain the weakening length scale within the subduction zone. The rate of drop off from the trench will depend on the mechanism of weakening, while other factors such as length of the slab, coupling of the slab to mantle flow (i.e., the magnitude of stress transmitted to the surface) and coupling along the plate boundary fault may also affect weakening of the subducting lithosphere. We have shown that by averaging parallel tracks from swath bathymetry data, the scatter in the response function is greatly reduced. This suggests that the spatial variation in the elastic strength of the lithosphere seaward of the subduction zone can be measured if appropriate data sets (ship tracks parallel to subduction

zones with swath bathymetry data) are available at a range of distances from the trench.

References

J. Aubouin, J. Bourgois, and J. Azema. A new type of active margin: the convergnet-extensional margin as exemplified by the Middle America Trench off Gautemala. *Earth and Planetary Science Letters*, 67:211–218, 1984.

David Bercovici. A source-sink model of the generation of plate tectonics from non-Newtonian mantle flow. *Journal of Geophysical Research*, 100:2013–2030, 1995.

J. H. Bodine and A. B. Watts. On lithospheric flexure seaward of the bonin and mariana trenches. *Earth and Planetary Science Letters*, 43:132–148, 1979.

Jean-Claude De Bremaecker. Is the oceanic lithosphere elastic or viscous? *Journal of Geophysical Research*, 82:2001–2004, 1977.

E. Carey and J. Dubois. Behaviour of the oceanic lithosphere at subduction zones: plastic tield strength from a finite-element method. *Tectonophysics*, 74:99–110, 1982.

J. R. Cochran. An analysis of isostasy in the world's oceans. A. Midocean ridge crests. *Journal of Geophysical Research*, 84:4713–4729, 1979.

Clinton P. Conrad and Bradford H. Hager. Effects of plate bending and fault strength at subduction zones on plate dynamics. *Journal of Geophysical Research*, 104: 17551–17571, 1999.

C. de Mets, R. G. Gordon, D. F. Argus, and S. Stein. Current plate motions. *Geophysical Journal International*, 101:425–478, 1990.

LeRoy M. Dorman and Brian T. R. Lewis. Experimental isostasy. 1. Theory of the determination of the Earth's isostatic response to a concentrated load. *Journal of Geophysical Research*, 73:3357–3365, 1970.

GEODAS. Geodas marine geological and geophysical data from U.S. Department of Commerce NOAA and NGDC. CDROM, 1992.

Anne V. Judge and Marci K. McNutt. The relationship between plate convergence and elastic plate thickness: a study of the Peru-Chile Trench. *Journal of Geophysical Research*, 96:16625–16639, 1991.

K. Kobayashi, J. P. Cadet, J. Aubouin, J. Boulegue, J. Dubois, K. Koizumi, S. Lallemand, Y. Nakamura, G. Pautot, K. Suyehiro, S. Tani, H. Tokuyama, and T. Yamazaki. Normal faulting of the Daiichi-Kashima seamount in the Japan Trench revealed by the Kaiko 1 cruise, leg 3. *Earth and Planetary Science Letters*, 83: 257–266, 1987.

Serge E. Lallemand, Michel Popoff, Jean-Paul Cadet, Anne-Gaelle Bader, Mauel Pubellier, Claude Rangin, and Benoît Deffontaines. Genetic relations between the Central and Southern Philippine Trench and the Sangihe Trench. *Journal of Geophysical Research*, 103:933–950, 1998.

C. Lithgow-Bertelloni, M. A. Richards, Y. Yicard, R. J. O'Connell, and D. C. Engebretson. Toroidal-poloidal partitioning of plate motion since 120 Ma. *Geophysical Research Letters*, 20:375–378, 1993.

Peter Lonsdale. A multibeam reconnaissance of the Tonga Trench axis and its intersection with the Louisville Guyot chain. *Marine Geophysical Researches*, 8:295–327, 1986.

D. G. Masson. Fault patterns at outer trench walls. *Marine Geophysical Researches*, 13:209–225, 1991.

Dan McKenzie and Carl Bowin. The relationship between bathymetry and gravity in the Atlantic Ocean. *Journal of Geophysical Research*, 81:1903–1915, 1976.

Marcia McNutt. Compensation of oceanic topography: an application of the response function technique to the Surveyor Area. *Journal of Geophysical Research*, 84:7589–7598, 1979.

H. J. Melosh. Dynamic support of the outer rise. *Geophysical Research Letters*, 5: 321–324, 1978.

R. J. O'Connell, C. W. Gable, and B. H. Hager. Toroidal-poloidal partitioning of lithospheric plate motion. In R. Sabadini, editor, *Glacial Isostasy, Sea Level and Mantle Rheology*, pages 535–551. Kluwer, Norwell, MA, 1991.

Yujiro Ogawa, Kazuo Kobayashi, Hiroshi Hotta, and Kantaro Fujioka. Tension cracks on the oceanward slopes of the northern Japan and Mariana Trenches. *Marine Geology*, 141:111–123, 1997.

D. T. Sandwell and W. H. F. Smith. Marine gravity anomaly from GeoSat and ERS1 satellite altimetry. *Journal of Geophysical Research*, 102(B5):10039–10054, 1997.

D. L. Turcotte, D. C. McAdoo, and J. G. Caldwell. An elastic-prefectly plastic analysis of the bending of the lithosphere at a trench. *Tectonophysics*, 47:193–208, 1978.

W. E. K. Warsi, T. W. C. Hilde, and R. C. Searle. Convergence structures of the Peru Trench between 10° s and 14∘ s. *Tectonophysics*, 99:313–329, 1983.

A. B. Watts. An analysis of isostasy in the world's oceans. 1. Hawaiian-Emperor Seamount Chain. *Journal of Geophysical Research*, 83:5989–6004, 1978.

A. B. Watts and S. F. Daly. Long wavelength gravity and topography anomalies. *Annual Reviews of Earth and Planetary Science*, 9:415–448, 1981.

A. B. Watts and M. Talwani. Gravity anomalies seaward of deep-sea trenches and their tectonic implications. *Geophysical Journal of the Royal Astornomical Society*, 36:57–90, 1974.

Shijie Zhong and Michael Gurnis. Interaction of weak faults and Non-Newtonian rheology produces plate tectonics in a 3-D model of mantle flow. *Nature*, 383: 245–247, 1996.